Atmósfera (1995), 8, *pp. 3-22*

Some statistical aspects of anthropogenic and natural forced global temperature change

CHRISTIAN–D. SCHÖNWIESE and DIETER BAYER

Institute for Meteorology and Geophysics, J. W. Goethe University, P. O. Box 111932, D–60054 Frankfurt/M., FRG

(Manuscript received Nov. 25, 1993; accepted in final form Aug. 15, 1994)

RESUMEN

Las fluctuaciones de temperatura observada globalmente cerca de la superficie a nivel hemisférico y meridional, zonalmente promediadas, en los periodos 1851-1991 ó 1861-1991, respectivamente, son reproducidas por modelos de regresión 'multiforzados' que toman en cuenta forzamientos volcánico, solar, ENSO y GHG (gases de invernadero). Más aún, las razones de las tendencias y tendencias respecto al ruido observadas se comparan usando fuentes de datos diferentes.

Las pruebas estadísticas diversas que incluyen forzamientos aleatorios de los datos libres de tendencia (prueba Monte Carlo) y extrapolaciones con base en los subperiodos de 'calibración' demuestran que el enfoque estadístico funciona muy bien. Por consiguiente, no sólo se presentan evaluaciones de las señales naturales y de gases de invernadero en series cronológicas de la temperatura observada, sino también extrapolaciones basadas en los escenarios A y D de la IPCC.

Una comparación con los resultados obtenidos a partir de simulaciones transitorias océano-atmósfera del Instituto Max Planck de Meteorología de Hamburgo, muestran una magnitud un poco mayor de las señales de GHG deducidas estadísticamente, en las que la diferencia, sin embargo, no es significativa cuando se toman en cuenta las incertidumbres de ambos métodos.

ABSTRACT

The observed global, hemispheric, and meridional (zonal means) temperature fluctuations near surface covering the period 1851-1991 or 1861-1991, respectively, are reproduced by 'multiforced' regression models which take into account volcanic, solar, ENSO, and GHG (greenhouse gases) forcing. Moreover, the observed trends and trend–to–noise ratios are compared using different data sources.

Different statistical tests including random forcing of detrended data (Monte Carlo testing) and extrapolations on the basis of 'calibration' subperiods demonstrate that the statistical approach works quite well. Therefore, not only assessments of GHG and natural signals in observational temperature time series are presented, but also extrapolations based on the IPCC scenarios A and D. A comparison with the results obtained from the Hamburg Max–Planck–Institute for Meteorology (MPI) coupled atmosphere–ocean transient simulations show a somewhat larger magnitude of the statistically derived GHG signals where the difference, however, is not significant when the uncertainties of both methods are taken into account.

1. Introduction and data base

Human activities lead to a concentration increase of atmospheric trace gases like carbon dioxide (CO_2), methane, chlorofluorocarbons and others. This process enhances the 'greenhouse effect': The tropospheric boundary layer near the surface is warmed by the increased infra–red absorption and reemission of GHG whereas the stratosphere is cooled by the decreased heat flux into the upper atmosphere. The preindustrial atmospheric CO_2 concentration is supposed to be 280 ± 5 ppm (Neftel *et al.*, 1985) compared to a Mauna Loa annual mean measurement of 355 ppm in 1991 (Keeling, 1982,1992; Houghton *et al.*, 1992). The contribution of additional GHG is usually expressed in terms of CO_2 equivalents. The 1991 combined estimate of CO_2 and CO_2 equivalents amounts of 412 ppm (Houghton *et al.*, 1992).

In contrast to the trace gas concentrations and the physical basis of the greenhouse effect, the definite climate response to the atmospheric GHG increase is a matter of considerable uncertainty. It is clear that the question of past and future GHG–forced global climate change should be primarily answered by sophisticated deterministic climate models simulating the coupled atmosphere–ocean–cryosphere circulation as realistic as possible including all relevant feedbacks (general circulation models, GCM). No doubt, there has been important progress in the development of such models in recent decades. However, there are still major deficiencies and most of them probably will remain in the next years. These problems concern all hydrological mechanisms (water vapour, clouds, precipitation, etc.), feedbacks (e.g. geochemical–biological), deep ocean circulation, sea ice movement and so on. It is not surprising, therefore, that even the probably most simple case, the prediction of the global mean surface air temperature rise in response to an atmospheric CO_2 doubling (compared to the preindustrial level), is uncertain: 2.7-4.5 K (equilibrium response) or 1.3-2.3 K (transient response); see IPCC, Houghton *et al.* (1992). Some scientists (e.g. Lindzen, 1990) argue that, due to hydrological problems, these assessments may be considerable overestimations although this conclusion is again uncertain. Figure 1 summarizes the IPCC transient assessments of the global mean temperature response to GHG forcing.

Another serious problem arises if these models are validated and verified against the present climate state and the observed past climate fluctuations. It is evident that the real climate is forced by a very manifold and complicated complex of both natural and anthropogenic forcing and that natural forcing has dominated in the past. While the uncertainties of observed monthly and annual means of surface air temperature over land areas of the recent roughly 100 years are fairly known and relatively small, their forcing is questionable. Only in a few simulations using drastically simplified climate models, mostly energy balance models (EBM), a 'multiforcing' was realized, e.g. by Hansen *et al.* (1981, 1988) or by Gilliland (1992) implying the CO_2, volcanic and solar influence on the global or hemispheric mean temperature.

Often GHG forced climate model simulations are compared with simply the overall observed climate change, e.g. global or hemispheric averages of surface air temperature, see again Figure 1, although observed temperature fluctuations are certainly not only GHG but multiforced. This aspect is underrepresented even in the IPCC Reports (Houghton *et al.*, 1990, 1992), particularly in their GHG signal detection issue. It is correct to say (IPCC) that all climate change observed in the past may have been natural or that, alternatively, the anthropogenic influence may have been larger than it is represented in past trends. It is stupid, however, to say that an only moderate temperature increase in the past and occasional cooling necessarily contradict GHG climate simulations. We simply do not know the details of multiforcing and there is an urgent need to improve this situation. One way to do this is a proper statistical analysis of climate observations and the evaluation of some forcing hypotheses and simple models using these statistical methods. All statistical hypotheses should be strictly related to a physical basis and their statistical

significance has to be tested. It is worth noting that statisticians applying and discussing these methods are dealing, in contrast to modellers, with observed data and therefore with reality.

Due to some observational advantages (fair accuracy and representativeness, fair reliability also for earlier time) and physical properties this paper is focussed on observed air temperature series, monthly and annual averages covering the instrumental period since 1851 at the maximum. In general, these considered series end in 1991. In case of the global mean temperature near surface we refer to the series used by IPCC (Houghton *et al.*, 1990, 1992), see Figure 1 (dotted line), land and marine data, provided by Jones *et al.* (1991, 1992). It should be noted that the sea surface temperature data incorporated in these series are very uncertain. Nevertheless, taking into account also the urbanization effect, IPCC states a < 0.1 K error of these annual mean data. Hemispheric mean averages are available again from Jones *et al.* (1991, 1992), additionally from Hansen and Lebedeff (1987, 1993), and from Vinnikov *et al.* (1990). Since these time series are very similar to each other (except the Hansen and Lebedeff data which

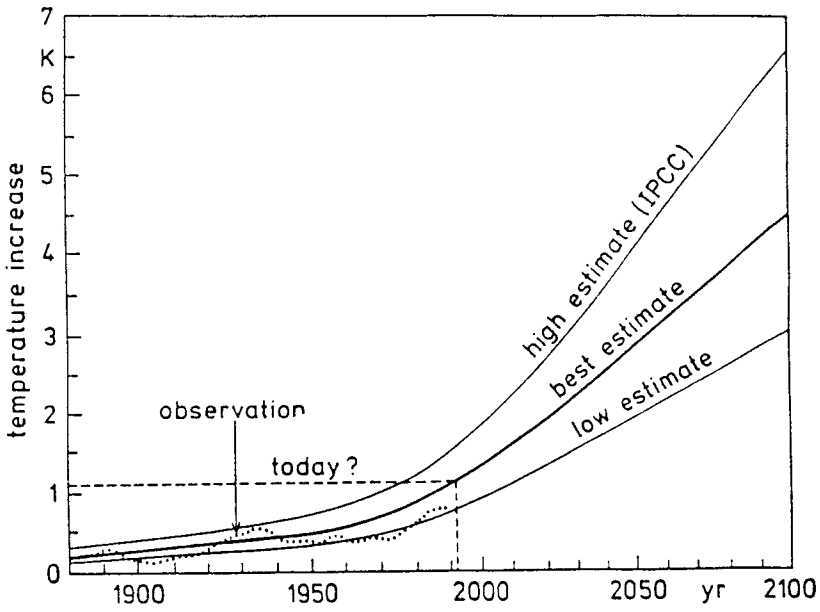

Fig. 1. Climate model assessments of global mean surface air temperature rise based on IPCC scenario A, from Houghton *et al.* (1990) and comparison with observations (again IPCC, land and marine temperatures, data from Jones (1992), 10 yr low-pass filtered).

reveal a somewhat larger Northern Hemisphere temperature increase 1891-1940) the Vinnikov data are omitted in Table 1 which compares the observed trends and trend-to-noise ratios. Two of these data sets are also available in a regional and seasonal (monthly) disintegration: The Jones *et al.* (1992) data refer to a 5° latitude/10° longitude grid focussed on land areas (details see Jones *et al.*, 1982) whereas the Hansen and Lebedeff (1993) data refer to 80 boxes each of equal area around the globe. We used a magnetic tape version where the globe is subdivided into 108 area components. Not all boxes or area compartments, however, are represented by temperature time series covering the total period under consideration, 1880-1985. So we used only 90°N-70°S boxes covering the period 1894-1985. As far as stratospheric temperatures are concerned we used mean hemispheric annual data from Angell (1988, 1992) which refer to the 100-30 hPa layer and from Labitzke *et al.* (1986, 1992) for the 30 hPa level. In agreement with the

greenhouse hypothesis all surface data records show long–term warmings and the stratosphere records show long–term coolings, see Figure 2. The oberved trends are, however, not uniform in time and space and there are considerable quantitative differences when GHG model projections and observations are compared.

TABLE 1. Trends and trend-to-noise ratios of mean hemispheric and global temperature series used in this paper.

Abbreviation	Explanation	Data source	Trend in K (trend-to-noise ratio) 1891-1990	1940-1970	1970-1990
TNH-J	Surface air temperature, northern hemisphere	Jones et al. (1991)	0.51 (2.08)	-0.23 (-1.53)	0.60 (2.23)
TNH-H		Hansen and Lebedeff (1987,1993)	0.53 (2.25)[2)]	-0.18 (-1.37)	0.36 (1.78)[3)]
TSH-J	Surface air temperature, southern hermisphere	Jones et al. (1991)	0.52 (2.59)	0.00 (0.00)	0.38 (2.04)
TSH-H		Hansen and Lebedeff (1987,1993)	0.37 (2.24)[2)]	-0.12 (-1.15)	0.22 (1.58)[3)]
TGLM	Global mean surface temperature[1)]	Jones et al. (1991)	0.44 (2.53)	-0.02 (-0.17)	0.38 (2.41)

[1)]sea surface temperatures included [2)]1891-1987 [3)]1970-1989

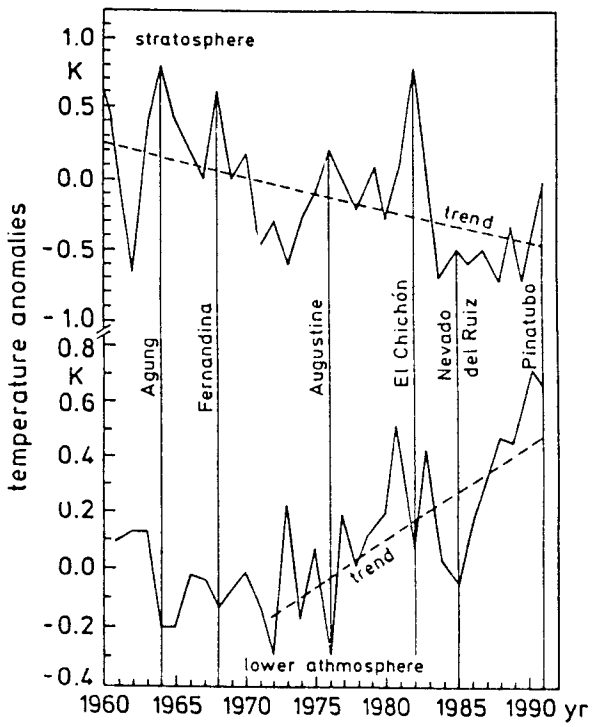

Fig. 2. Comparison of observed mean Northern Hemisphere annual temperature anomalies, 1960-1991 in the stratosphere (data from Labitzke *et al.*, 1986-1992) and in the atmosphere near surface (data from Jones 1991, 1992), including linear trends. Some explosive volcanic eruptions are also indicated.

In consequence, in many earlier papers some forcing parameters have been discussed which may be in competition with the enhanced greenhouse effect (Robock, 1979; Gilliland, 1982; Hansen *et al.*, 1981, 1988; Houghton, 1990, 1992; Miles and Gildersleeves, 1978; Schönwiese, 1983; Schönwiese and Runge, 1991; Schönwiese and Stähler, 1991). Competition means that the scale in both time and space is comparable to that of GHG forcing. This means, we have to look at mechanisms influencing the global climate and operating on time scales of decades and centuries. Usually one concentrates on mechanisms acting as external forcing on the climate system, but oceanic processes or atmosphere–ocean interactions should not be neglected.

One of the external mechanisms is volcanism: Explosive eruptions causing particle loadings of the stratosphere (including gas–to–particle conversions) are known to be of important climatic relevance. This has been analysed in a number of case studies and in more general aspects by means of EBM or radiative convective (RCM) climate models. Figure 2 illustrates the simultaneous temperature behaviour by means of observational data of the Northern Hemisphere after major explosive volcanic eruptions where the warmings (stratosphere) and coolings (near surface are clearly indicated in most cases. Lamb (1970, 1983) has done some pioneer work in evaluating hemispheric annual volcanic activity parameter time series, see also Robock (1991); Lamb's volcanic 'dust veil index' DVI, see Table 2, has been broadly used. Another proxy parameter is available from Greenland ice core measurements (volcanic acid deposition) called 'acidity index' AI (Table 2). Schönwiese (1988a, 1988b) as well as Cress and Schönwiese (1990, 1992) have tried to evaluate an additional volcanic activity parameter time series based on the Simkin *et al.* (1981, 1989) volcano chronology (Smithsonian Institution, USA) and they called their data 'Smithsonian (based) volcanic index' SVI which is available for the whole globe (SVIG), for the northern (SVIN), and for the Southern Hemisphere (SVIS), each in two versions, where SVI*G, SVI*N, and SVI*S take account for the stratospheric particle residence time assessed by SVI–AI intercomparisons. The different volcanic activity parameters imply certain advantages and disadvantages and their intercorrelations are relatively small (Cress and Schönwiese 1990, 1992, Schönwiese 1988a). So, it is appropriate to use these parameters alternatively instead of

TABLE 2. Natural forcing parameter time series (annual) used in this paper.

Type	Abbreviation	Explanation	Data source
Volcanic	AI	Acidity index, ice cores	Hammer et al. (1980)
	DVI	Dust veil index, stratosphere	Lamb (1983)
	SVI	Smithsonian (Inst. based) volcanic activity index	Simkin et al. (1981,1989), Cress and Schönwiese (1992)
	SVI*	Similar, but stratospheric particle residence time incorporated	Simkin et al. (1981,1989), Cress and Schönwiese (1992)
Solar	SCL	Solar cycle length (≈11yr)	Friis-Christensen and Lassen (1991)
	SDT	Solar diameter derived temperature variations	Gilliland (1982)
	SHM	Sunspot derived solar constant variations[1)]	Hoyt (1979); modified by Schönwiese (Schönwiese et al. 1992)
	SKN	Similar[1)]	Kondratyev (1970)
	SOC	Solar constant variations derived from satellite measurements[2)]	Foukal and Lean (1990)
	SRN	Sunspots	
ENSO	ENW	El Niño, Pacific SST	Wright (1984)
	ENS	El Niño, Pacific SST	Schneider and Schönwiese (1989)
	SO	Southern oscillation index	Jones (1991)

[1)]Hypothetical [2)]Close correlation with SRN

preferring any particular one. Furthermore, it is important to check the coherences with temperature (Fig. 3). This statistical aspect reveals that correlations in the long–term domain of the variance spectrum are more pronounced than in case of singular events (year–to–year correlations). Unfortunately long–term time series of the stratospheric sulfate concentration (which is more climate–relevant than stratospheric dust) were not available until very recent time (Dai, 1992). This new information will be used in our future work.

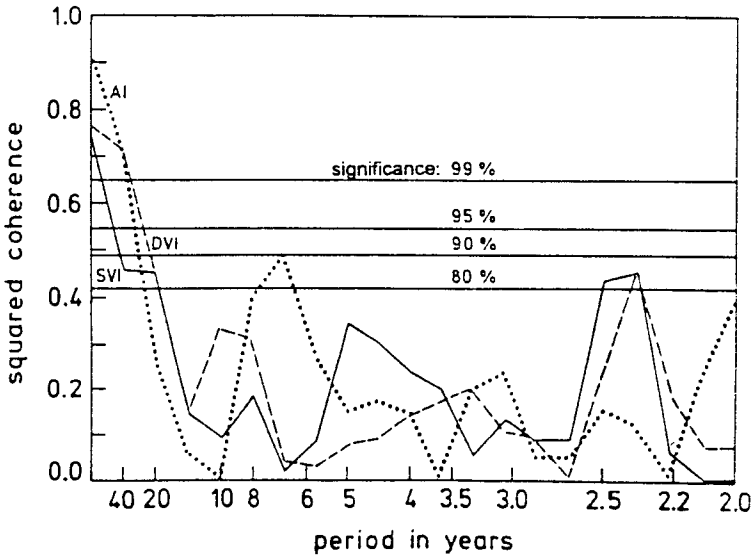

Fig. 3. Coherence (squared) spectra of observed mean Northern Hemisphere annual temperature, 1881-1980 and the volcanic activity parameter time series indicated (see Table 2); from Schönwiese (1988a).

The solar signal in climate is a matter of controverse discussion. Similar to volcanism–climate relationships Schönwiese *et al.* (1992, 1994) have also dealt with solar–climate aspects. An important fact is the variation of the solar constant within the recent roughly 10 years and its correlation with sunspots (Lee *et al.*, 1988, 1990) although the magnitude of this variation amounts to no more than 0.1%. Following model simulations of Hansen *et al.* (1988) this should lead to a response in the global mean surface air temperature of 0.07 K. If the hypothesis is accepted that, on a time scale of centuries, solar activity undergoes larger variations (Eddy, 1967, Eddy *et al.*, 1982) than in the recent decade, a response of a few tenths of a degree may be possible. The solar parameter time series used alternatively in this study are listed in Table 2. Most of them are related to sunspot relative numbers, including these numbers themselves, satellite–based conversions into solar 'constant' variations and variations of the length of the quasi–eleven–year–cycle. A more or less alternative possibility is the solar diameter variation hypothesis of Gilliland (1982) in terms of a radiative forcing parameter time series or a time series describing the temperature response derived from EBM simulations. Additional hypotheses, for example based on gravitudinal effects of the big planets on the sun (Landscheidt, 1988) reveal so poor correlations with temperature that they are neglected.

The ENSO (El Niño/southern oscillation) mechanism can be described by tropical Pacific SST anomalies (El Niño) or the Tahiti-Darwin surface air pressure difference index (southern oscillation, SO) which is used here (Jones, 1991). In contrast to the other forcings considered in this study, spectral analyses reveal that the ENSO variance is dominating on a year–to–year time scale (Schneider and Schönwiese, 1989) and that the coherence with temperature shows no significant relationship on time scales of decades or centuries.

GHG forcing was often simulated by a variety of climate model experiments as mentioned above. From the statistical point of view it is reasonable to suppose that related forcing parameter time series (CO_2 or CO_2 equivalents) may be proportional to the temperature response. The simplest way to prove this hypothesis is to assume, in a first approach, a linear relationship. Augustsson and Ramanathan (1977), however, have shown that the CO_2 main absorption band near 15μm causes a logarithmic temperature response. Other, weaker CO_2 absorption bands show a linear relation. Due to the relatively small CO_2 concentration increase observed within the last century it appears that the relation with temperature can be approximated adequately in a linear way. For future scenarios assuming a much larger GHG concentration increase, however, it is appropriate to use the logarithmic relationship.

2. Design of the multiforced statistical model

a. Some basic considerations

The multiforced statistical model used in this paper is based on the physical background outlined in section 1. These physical relationships imply the statistical expectation that observed surface air temperature variations are positively correlated with the GHG concentrations, solar, and ENSO forcing whereas in case of volcanic activity negative correlations are expected. Considering stratospheric temperatures, all these correlations should change their sign. In consequence, first of all uniforced correlations and, introducing possible phase shifts of cause and effect, cross correlation coefficients have to be computed. This has been done in a series of previous work (e.g. Schönwiese, 1983; Schönwiese, 1991; focussed on volcanic forcing, see Cress and Schönwiese, 1992; Schönwiese, 1988a; focussed on solar forcing see Schönwiese *et al.*, 1992, 1994). Therefore, in this paper it may be sufficient to summarize the order of magnitude. In respect to the recent 100-140 years and analysing unfiltered annual means, the volcanic correlation coefficients amount to approximately -0.3 to -0.4, with phase shifts of 1-5 years for the Northern Hemisphere and -0.2 to -0.3 for the Southern Hemisphere; t–tests (where, of course, autocorrelations are taken into account by reduced degrees of freedom) reveal high significance (95-99% corresponding 0.05-0.01 error probability) for the Northern and weak significance ($\sim$ 90%) for the Southern Hemisphere. Rank instead of Pearson correlations coefficients and the Fisher transformation for non–Gaussian distributed quantities lead to very similar results, also in case of solar, ENSO, and GHG forcing.

In respect to solar forcing, the problem arises that (much more than in case of volcanic forcing) the correlation coefficients are not stable in time. Based on the recent 100 years SRN (abbreviations see Table 2) correlations fluctuate around +0.3, and are significant at 90-95% levels (0.1-0.05 error probability). SHM and SOC (+0.3 to +0.4) and especially SCL (+0.4 to 0.5) correlations are somewhat more established and very similar for the Northern and Southern Hemisphere whereas SDT correlations show some hemispheric differences (c.+0.4 for the Northern and c.+0.3 for the Southern Hemisphere); SKN correlations are not significant. Using proxy data for the Northern Hemisphere surface air temperature reconstructions (data source Jacoby and D'Arrigo, 1989), SDT correlations drop to -0.1 to 0.1 and are no longer significant and SCL correlations drop to 0.2 (weak significance) whereas SRN correlations (0.2 to 0.3) remain highly significant (99%). (In case of SCL the cycle length is negatively correlated with solar activity, see Friis–Christensen and Lassen, 1991; we have changed the sign in order to expect positive correlations in case of all solar forcing).

ENSO forcing reveals correlation coefficients (recent 100 years) of approximately +0.2 (significance 95%) for the Northern and +0.3 (significance 99%) for the Southern Hemisphere. Cross correlations indicate no significant phase shifts.

GHG correlations are extremely questionable because this forcing implies no fluctuations. The correlations are in the order of +0.6 to +0.7 and despite extreme autocorrelation significant at the 99% level. It is supposed, however, that the automatic application of statistical test procedures fails to reveal reliable results in case of GHG forcing (further discussion see section 2b).

All correlations except ENSO increase if 10 yr, 20 yr, etc.; low–pass filtered data are used but, due to increasing autocorrelation, these relationships lose their significance in this case. Coherence analysis, however (see examples given in Fig. 3), is appropriate to show that in respect to all except ENSO forcing long–term correlations are more pronounced than year–to–year correlations where random forcing may contribute a considerable amount of variance. Stratospheric data reveal, due to very short observation periods, only weak correlations and are, therefore, neglected in the following.

b. Strategy and Monte Carlo testing

The basic idea of the strategy which aims at the reproduction and hypothetical explanation of a dominant part of the observed climatic variance and, furthermore, the hypothetical detection of the enhanced greenhouse effect in observations is that the observed climatic variance comprises an only weak stochastic component (random and other unknown or not considered forcing); some major part of the observed variance may be forced by natural processes like volcanism, etc.; finally, we look on the GHG forced signal which should be detected as early as possible. Filtering in space (using large–scale averages, up to a hemisphere or global mean) and time (low–pass, smoothing) may eliminate some part of the stochastic variance. Concerning the remaining both natural and anthropogenic variance, the simplest statistical approach is a linear regression equation

$$t = a_o + a_1 V + a_2 S + a_3 E + a_4 G \tag{1}$$

where t is any climatic element, in this paper surface air temperature, V any (alternative!) volcanic parameter, S any (again alternative) solar parameter, E any ENSO parameter, and G greenhouse forcing, all annual or, in case of t also seasonal data, unfiltered or low–pass filtered. Using this concept one has to check whether such a simple regression model is able to reproduce a predominant part of the total observed climatic variance. Although all considered forcing parameters are strictly based on physical relationships and although their statistical significance has been checked by cross correlation and coherence analyses, including usual tests, the reproduction of the observed climatic variance by this statistical multiforcing may be by chance. In order to check this possibility, we performed a Monte Carlo testing using, in respect to the recent 100 yr mean Northern Hemisphere surface air temperature (annual means), a random forcing. For this purpose we eliminated the major part of autocorrelation from the climatic data by high–pass filtering and computed the multiple correlation coefficients r_m from forcing by three random series R_i

$$t = a_o + A_1 R_1 + a_2 R_2 + a_3 R_3 \tag{2}$$

where t, R_1, R_2, R_3 are again time series. This has been done in 1000 different combinations of random series and the results are shown in Figure 4. The absolute r_m (multiple correlation coefficients) frequency distribution shows a maximum at $r_m = 0.10 - 0.13$; r_m values > 0.33

did not appear (Fig. 4a). The corresponding relative frequency distribution (Fig. 4b) indicates that $r_m > 0.3$ means $> 99\%$ (error probability < 0.01) and $r_m > 0.33$ means $> 99.9\%$ (error probability < 0.001) significance of the multiforced statistical regression model. Then we did the same using all combinations of V, S and E (see Table 2) forcing and found an r_m range of 0.58 to 0.63. So, our statistics 'explaining' natural variability is highly significant although we do not know which combination of natural forcing parameters may be the best one on a physical basis. We assume that SVI*, SOC, and SO may be appropriate from this point of view and discuss, in the following, this combination called 'alternative model' in contrast to the 'best fit model' (SVI*, SDT, SO) combination which reveals the maximum multiple correlation coefficient.

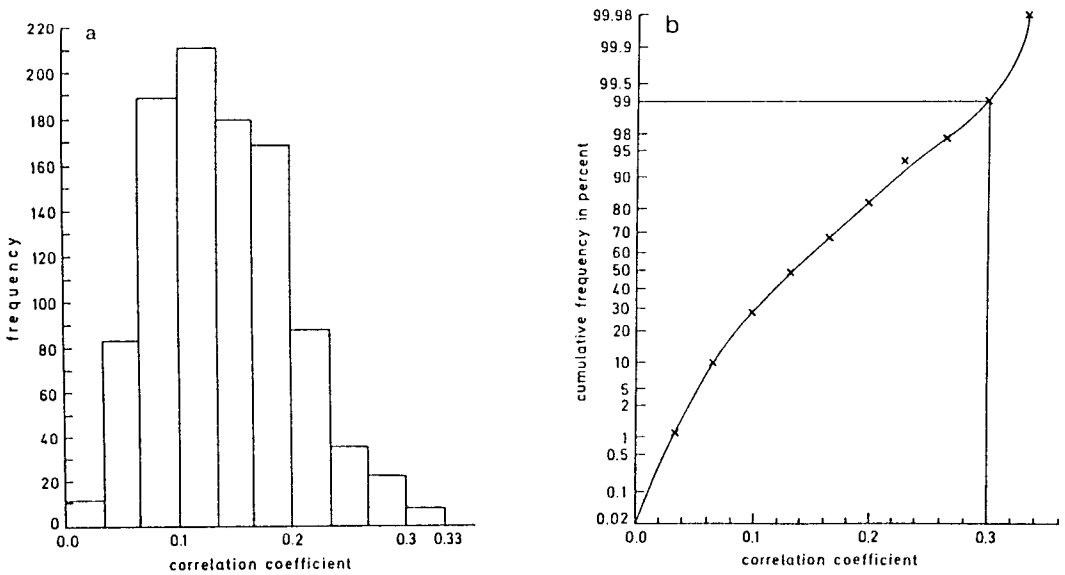

Fig. 4. (a) Frequency distribution of multiple correlation coefficients arising from the analysis of mean Northern Hemisphere annual temperatures 1881-1980 as described in the text (Monte Carlo testing, 1000 combinations of random forcing, temperature data detrended). (b) Corresponding cumulative frequency distribution. From Schönwiese (1994).

Adding GHG forcing and, simultaneously, autocorrelation (as observed) to the climate data time series, the multiforced statistical regression model has to be tested whether it explains significantly more variance as would be due to autocorrelation. Furthermore, r_m values should be checked by usual F–tests. A third independent method is to isolate the singals from the statistical model which are due to particular forcing and to compare these signals with corresponding results from deterministic climate models. For instance, GHG signals which may have been realized so far as available from

$$S = a_4(G_2 - G_1) \tag{3}$$

where G_1 may be the preindustrial CO_2 concentration (280 ppm) and G_2 the present value (or corresponding CO_2 equivalents). Note that this way of statistical signal assessment aims at the temperature effect of one isolated forcing factor but, at the same time, uses the regression coefficient a_4 of the multiple model. Such signals, therefore, are different from those derived from an uniforced correlation and signal analysis.

In contrast to natural forcing, however, where fluctuations dominate, GHG forcing is characterized by a continuous trend and usual GCM projections refer to future situations. In order to enable intercomparisons of statistical assessments as suggested in (3) with GCM projections it is necessary to amplify the signals identified in the observations so far. Because the statistical regression model is calibrated for the observation and not for a future period, it is necessary to base the statistical extrapolation (using e.g. $G_1 = 280$ ppm or 300 ppm and $G_2 = 600$ ppm in (3)) on further informations as discussed in section 1 leading to a logarithmic GHG–temperature relationship.

A dilemma, however, should be noted concerning filter techniques. Filtering in space, especially in case of hemispheric or global averages, does not allow to look at seasonal and regional signal patterns known as multivariate (different climatic elements or one element at different locations simultaneously considered) or 'fingerprint' method. It is necessary, therefore, to look at both large–scale averages and regional patterns. Filtering in time may diminish stochastic variance but, at the same time, increases autocorrelation. It is reasonable, therefore, to look at both low–pass filtered data (in this paper in general 10 yr Gaussian low–pass filter) which represent a dominant part of explained variance and unfiltered data in the context of statistical testing.

In principle, (1)-(3) can be applied also on station or gridpoint data so that every station or gridpoint is represented by its typical set of regression coefficients for the reproduction of observed climatic change. The same holds for seasonal and monthly considerations.

3. Hemispheric and global mean reproductions of observed temperature fluctuations

Figure 5 shows the 10 yr low–pass filtered observed surface air temperature fluctuations, Northern or Southern Hemisphere or global averages, solid lines, the statistical best fit reproductions, dashed lines, the alternative reproductions, dashed–solid lines, and the GHG signals (based on CO_2 equivalents) derived from the alternative model, dotted lines. Table 3 specifies the characteristical statistics of these simulations where all testing refers to unsmoothed annual data (plots not shown). The time lags used are 20 yr in case of GHG, 5 yr (best fit) or 1 yr (alternative) in case of volcanic, and 1 yr (best fit) or 0 yr (alternative) in case of solar forcing. ENSO forcing is incorporated unshifted into the annual data reproductions and testing. According to (1) the best fit regression equations are given by

$$t = -20.09713 - 0.00031\ \mathrm{SVI^*N} + 0.00087\ \mathrm{SDT} - 0.02806\ \mathrm{SO} + 3.50711\ \ln(\mathrm{GHG}) \quad \text{(Northern Hemisphere)}$$
$$t = -22.08424 - 0.00023\ \mathrm{SVI^*S} + 0.00041\ \mathrm{SDT} - 0.07241\ \mathrm{SO} + 3.83881\ \ln(\mathrm{GHG}) \quad \text{(Southern Hemisphere)}$$
$$t = -19.03732 - 0.00016\ \mathrm{SVI^*G} + 0.00049\ \mathrm{SDT} - 0.05013\ \mathrm{SO} + 3.31394\ \ln(\mathrm{GHG}) \quad \text{(global)} \qquad (4)$$

For the alternative model we get

$$t = -63.89076 - 0.00018\ \mathrm{SVI^*N} + 0.03128\ \mathrm{SOC} - 0.04240\ \mathrm{SO} + 5{,}68245\ \ln(\mathrm{GHG}) \quad \text{(Northern Hemisphere)}$$
$$t = -135.04578 - 0.00027\ \mathrm{SVI^*S} + 0.08529\ \mathrm{SOC} - 0.07734\ \mathrm{SO} + 3.20408\ \ln(\mathrm{GHG}) \quad \text{(Southern Hemisphere)}$$
$$t = -54.46433 - 0.00014\ \mathrm{SVI^*G} + 0.02639\ \mathrm{SOC} - 0.05721\ \mathrm{SO} + 3.19828\ \ln(\mathrm{GHG}) \quad \text{(global)} \qquad (5)$$

Evidently the statistical model works quite well. Note that, for instance, the Northern Hemisphere cooling between roughly 1940-1970 (best fit model) and other fluctuations are fairly

reproduced. The multiple correlation coefficients r_m amount to 0.90-0.95 in case of low–pass filtered and 0.7-0.9 in case of unfiltered annual data. Similar to Monte Carlo testing described in section 2b also F–testing reveals highly significant results. The GHG signals in the global

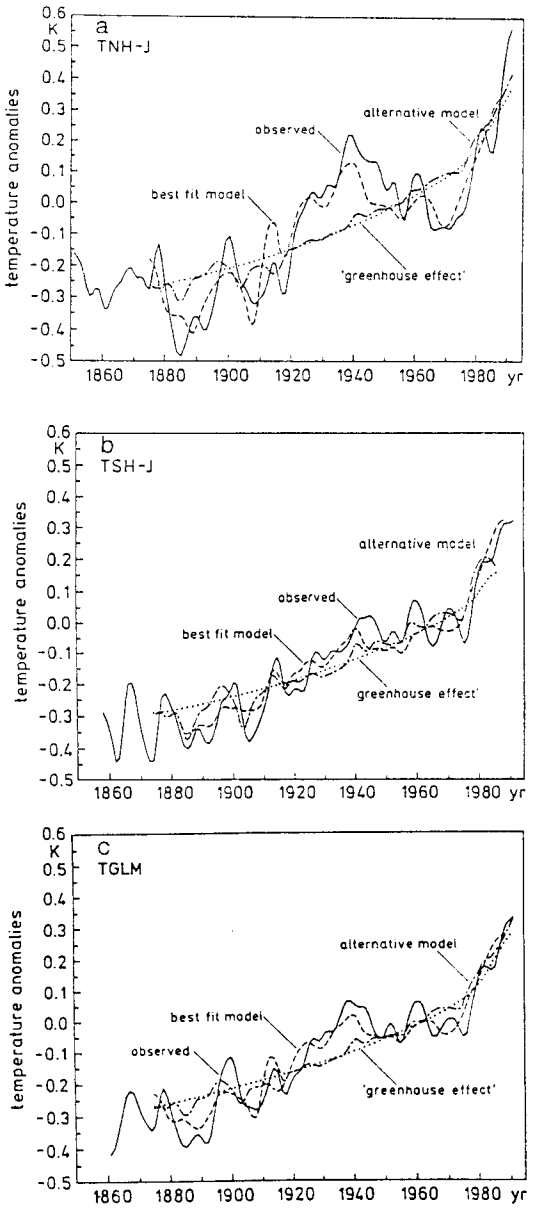

Fig. 5. (a) Observed mean Northern Hemisphere surface air temperatures 1851-1991 (data from Jones, 1992), 10 yr low–pass filtered, solid line, reproduction by the best fit version of the multiforced regression model described in the text, dashed line, reproduction by the alternative model, dashed–solid line and assessment of the enhanced GHG signals by means of this model, dotted line; see also Table 3. (b) Similar to (a) but Southern Hemisphere, 1858-1991. (c) Similar to (a) but global mean temperature 1861-1991 (surface air and marine data, IPCC).

TABLE 3. Some characteristical statistics to Figure 5: GHG signals (trends) in observed temperatures, multiple regression models (best fit versions); abbreviations of time series see Table 1.

Temperature record	Autocorrelation	Multiple correlation	F-Test (significance level)	GHG signal until 1990 (uncertainties)
TNH-J	0.66	0.77	> 99 %[1)]	0.7 K (-0.1 K/+0.1 K)
TNH-H	0.80	0.83	> 99 %[2)]	0.9 K (-0.1 K/+0.2 K)
TSH-J	0.71	0.83	> 99 %[3)]	0.7 K (-0.1 K/+0.1 K)
TSH-H	0.66	0.79	> 99 %[3)]	0.5 K (-0.0 K/+0.2 K)
TGLM	0.81	0.85	> 99 %[1)]	0.7 K (-0.1 K/+0.1 K)

[1)]sample size n=115 [2)]sample size n=112 [3)]sample size n=105

mean temperature since preindustrial times (280 ppm) until 1990 (354 ppm) are 0.6-0.8 K (CO_2 equivalents) or 0.4-0.6 K (only CO_2 forcing); corresponding signal time series (see Schönwiese, 1991). Some previous work (Malcher and Schönwiese, 1987; Schönwiese and Runge, 1991) has shown that these correlations and signals are broadly independent from the underlying temperature data sets (Vinnikov *et al.*, 1990 or Hansen and Lebedeff, 1987 instead of Jones *et al.*, 1991, 1992) and variations of the underlyng period (see Malcher and Schönwiese, 1987) except if proxy data are used (Schönwiese, 1992).

4. Stability aspects

This change of the underlying period considered, however, was not performed systematically in our earlier work. In particular, one may define any calibration period as a subperiod of all available observations and look at the statistical simulations in case of backward (reproduction, similar to some paleoclimatological methods) and forward (prediction) extrapolations. Examples for such procedures are shown in the Figure 6 (backward as well as forward extrapolation). Obviously the length of the calibration period should not fall below a certain value. Otherwise typical characteristics of any forcing parameter may be lost leading to considerable misinterpretations. An instructive example of such an error are the simulations drawn in Figure 6a. The curve called 'complete simulation' is the statistical best fit reproduction of the global mean temperature based on the regression interval from 1875 to 1987. The other four simulations are backward extrapolations, all including reduced regression time intervals ending in 1987. Evidently, the simulations with regression intervals beginning after 1919 show some considerable anticorrelations after periods of strong volcano activity. This is because those time intervals contain no or only weak volcanic eruptions so that, due to lack of information, the model is not able to respond correctly. Common to all extrapolations shown in the Figure 6 is an overestimation of the actually observed temperature. This can be traced back to the fact that in the backward extrapolation case the model 'knows' the 1940-1970 temperature decrease while in the forward extrapolation case the model does not.

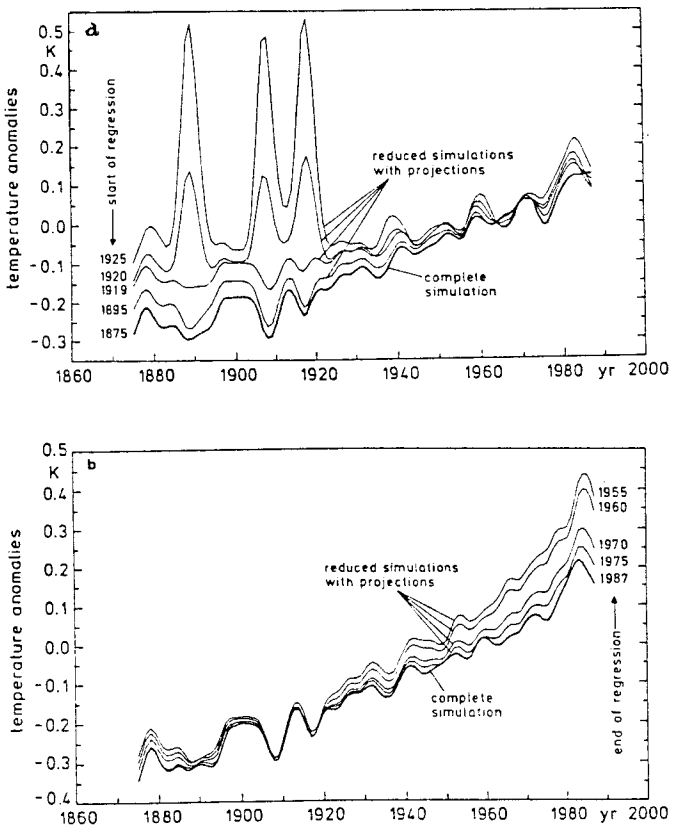

Fig. 6. (a) Complete (1875-1985) as well as reduced regression simulations (each up to 1987) with backward extrapolation of the regression equation back to 1875. (b) Complete (1875-1987) as well as reduced regression simulations (each starting 1875) with forward extrapolation of the regression equation up to 1987.

5. Overview of natural signals

As mentioned above, a further test of the statistical model is its ability to reproduce signals from natural forcing to an acceptable degree. Here we concentrate again on hemispheric and global means; for a discussion of seasonal–regional signals arising from volcanic or solar forcing see Cress and Schönwiese, 1992 or Schönwiese *et al.*, 1992, 1994, respectively.

Table 4 summarizes the surface air temperature signals which may have been forced by volcanic, solar or ENSO influence. These signals are maximum temperature effects which can be identified from annual or 10 yr low–pass filtered data in the period under consideration (method see (3)). For the Northern Hemisphere the maximum volcanic absolute signals range from 0.1 to 0.45 K. A global mean best estimate may be 0.3 K. This is very close to the number found by Hansen *et al.* (1981, 1988) on the base of deterministic climate modelling. If one analyses longer periods including proxy data (Schönwiese, 1988a, 1992) this signal assessment does rather decrease a little bit than increase. The solar signals reveal a much larger variety in respect to underlying periods and forcing parameters. Based on the recent 100-140 yr SRN and SOC signals indicate a magnitude < 0.1 K compared to $+0.3$ to $+0.4$ K for SCL and SDV forcing. For longer periods SRN and SCL signals show roughly the same magnitude $+0.1$ to $+0.4$ K, whereas SDV signals are negligible. A global mean best estimate may be $+0.1$ K for the recent 100 and

TABLE 4. Some assessments of maximum natural signals (amplitudes) in surface temperature, multiple regression models; time series see Tables 1 and 2.

Temperature record	Mechanism	Mean max. absolute signal (mean max. absolute signal-to-noise ratio)	Range of max. absolute signals from all regressions
TNH-J	Volcanism	0.24 K (0.94)	0.10 K - 0.38 K
	Solar	0.18 K (0.71)	0.02 K - 0.40 K
	ENSO	0.15 K (0.59)	0.11 K - 0.19 K
TNH-H	Volcanism	0.26 K (0.95)	0.08 K - 0.45 K
	Solar	0.18 K (0.68)	0.00 K - 0.41 K
	ENSO	0.15 K (0.56)	0.11 K - 0.19 K
TSH-J	Volcanism	0.13 K (0.65)	0.07 K - 0.29 K
	Solar	0.11 K (0.53)	0.04 K - 0.19 K
	ENSO	0.28 K (1.40)	0.25 K - 0.30 K
TSH-H	Volcanism	0.11 K (0.66)	0.03 K - 0.30 K
	Solar	0.11 K (0.61)	0.00 K - 0.24 K
	ENSO	0.22 K (1.24)	0.20 K - 0.24 K
TGLM	Volcanism	0.13 K (0.72)	0.03 K - 0.22 K
	Solar	0.09 K (0.49)	0.00 K - 0.22 K
	ENSO	0.20 K (1.08)	0.18 K - 0.23 K

+0.2 K for the recent 200-300 years. This is in fair agreement with the results from Hansen *et al.* (1981, 1988) if one is aware of the fact that the real variations of the solar 'constant' may be in a 0.1% order of magnitude rather than 1% as simulated by Hansen *et al.* (1988).

6. Extrapolations based on IPCC scenario A and D

Keeping in mind all restrictions and problems arising in the application of the statistical regression model (namely, uncertainty concerning data, inhomogeneity of data density, variety of natural forcing parameter data time series, uncertainty concerning the CO_2 equivalent concept, uncertainty concerning the nonlinearity between forcing and temperature response (all section 1), low–pass filter problems (section 2) and stability problems (section 4)) scenarios of future climate trends can be studied. The IPCC (Houghton *et al.*, 1990) scenarios A and D are broadly known, describing two future CO_2 equivalent concentrations. Scenario A ('business–as–usual') supposes a trace gas doubling occurring around the year 2025 while scenario D ('accelerated policies') assumes a stabilization of the GHG concentration within the next 100 years. Using time–averaged values for the natural forcing parameter data, extrapolations based on the GHG scenarios A and D, aiming at describing the global mean temperature effect, can be computed by (3). Figure 7 shows the resulting statistical temperature signals of a best fit simulation (regression interval 1875-1987), with Figure 7a assuming IPCC scenario A and Figure 7b IPCC scenario D (dashed lines). In both assessments a logarithmic relationship between GHG forcing and temperature was used. The error bars include assessments using different combinations of other than GHG influence parameter time series. The solid lines show the global mean annual surface air temperature variations as observed (TGLM according to Jones; Table 1) for the period of 1861-1985, and from 1985, according to the results of the transient IPCC GCM simulation of the MPI (Cubasch *et al.*, 1991, 1992). Note that the GCM simulations may underestimate the climate response by up to 0.5 K due to systematical error (Sausen *et al.*, 1992). In case of the GHG doubling scenario A the multiple regression model leads to an increase of 1.7 K in the global mean surface air temperature (referred to the 1985 value; see Table 5), which is exactly the IPCC best estimate. Including the 0.5 K error of the GCM simulations this value also corresponds to the MPI results. In case of the IPCC scenario D the GCM temperature rises within 100 years by less than 1 K, while the statistical model predicts a 1.6 K (IPCC: 1.2 k) increase. Again, considering the GCM error, all models correspond rather well.

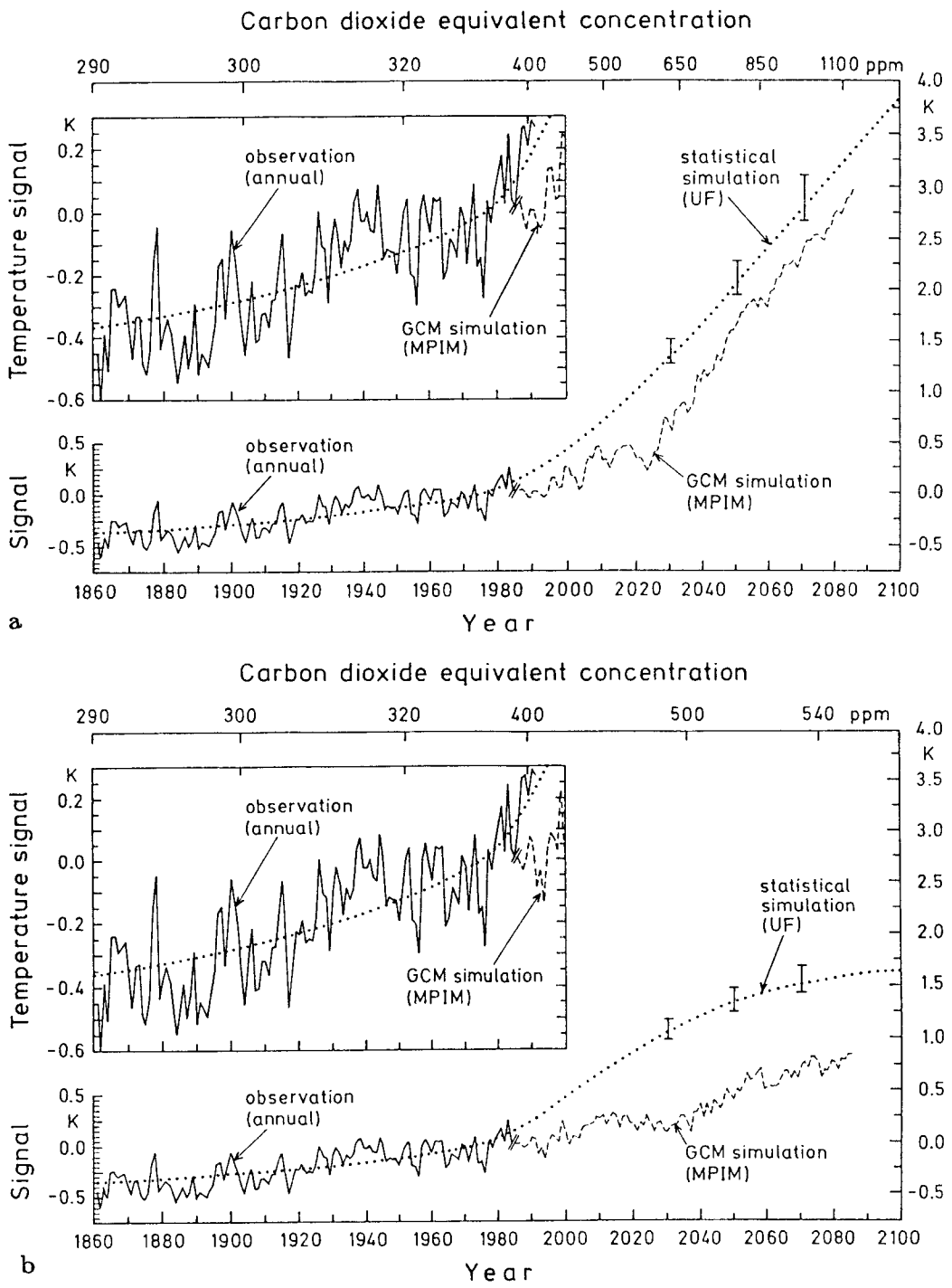

Fig. 7. (a) Observed global mean annual surface air temperature variations, 1861-1985 (upper plot 1861-1991), transient IPCC scenario A GCM simulation 1985-1085 (solid line), and corresponding statistical assessments of the greenhouse temperature signal with logarithmic GHG–tempeature relations (dashed line): upper plot ordinate scale amplified. All temperature signals refer to the 1985 value. Error bars include assessments using different combinations of forcing parameter time series. (b) Similar to (a) but transient IPCC scenario D GCM simulation.

TABLE 5. Future GHG signals based on IPCC scenario A, see Figure 7a.

Reference year	Actual year	Signal	Uncertainty
Preindustrial (≈1800)	1990	0.7 K	-0.1 K/+0.1 K
1985	2025	1.1 K	-0.1 K/+0.1 K
1985	2045	1.7 K	-0.1 K/+0.1 K
1985	2085	3.4 K	-0.2 K/+0.2 K
1985	2100	3.9 K	-0.3 K/+0.2 K
Preindustrial (≈1800)	2100	4.5 K	-0.3 K/+0.2 K

7. Seasonal and regional assessments

With regard to the spatial and seasonal response pattern, the statistical assessment are again in fair agreement with many deterministic models (Houghton *et al.*, 1990): The largest GHG-induced temperature signals can always be detected in the arctic winter. Figure 8a specifies the seasonal and meridional feature (zonal averages) of the 'industrial' temperature response due to a CO_2 concentration increase from 280 to 350 ppm, as revealed by the linear statistical regression model based on the Hansen and Lebedeff (1987) 108 box data set. Because of the poor data density in the Southern Hemisphere no reliable results can be obtained for the area south of 60°S. Nevertheless, the statistical calculations indicate a considerable temperature increase also in the southern polar winter. Applying a logarithmic instead of the linear trace gas–temperature relation, neither the seasonal–spatial pattern nor the magnitude of the industrial temperature response changes remarkably (Schönwiese and Stähler, 1991).

The situation changes if the signals of linear and logarithmic future extrapolations in respect to a trace gas concentration doubling are compared: Figure 8b shows the temperature pattern (again zonal averages) which appears as an extrapolation of the linear regression model results (data base 1890-1985) to CO_2 concentration doubling (see the procedure as described in section 2). A temperature signal of 5 K is calculated for the northern winter at 50°N. In the arctic

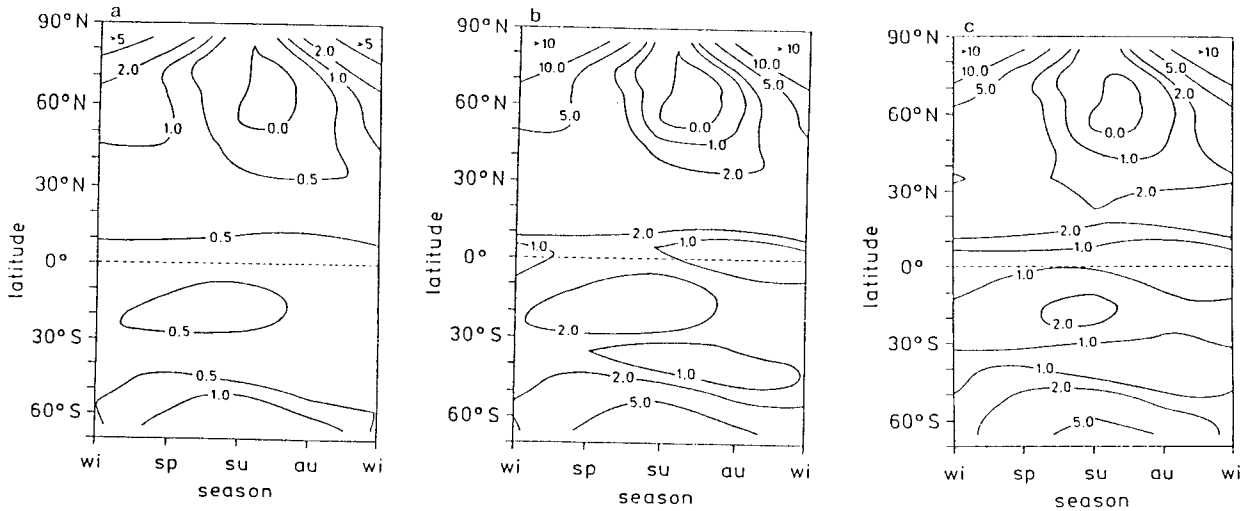

Fig. 8. (a) 'Industrial' (CO_2 concentration increase 280 to 350 ppm forcing) surface air temperature signals in K, zonal averages, as assessed by the statistical regression model described in the text; north-hemispheric seasons. (b) similar to (a) but extrapolation of the linear regression model results to CO_2 concentration doubling. (c) Similar to (a) but extrapolation of the logarithmic regression model results to CO_2 concentration doubling.

winter the signals exceed 10 K. The corresponding logarithmic regression model extrapolation reveals (with exception of the equatorial region and the northern summer) a lower magnitude of the temperature signals, while the seasonal and meridional structure is preserved (Fig. 8c). The 5 K signal limit in the northern winter, for example, in this case moves northward by 13° to 63°N. For reasons discussed in section 1 the logarithmic approach leading to lower trace gas doubling signals seems to be more realistic.

8. Conclusion

Multiforced regression models based on observational temperature data are able to reproduce both a major part of natural fluctuations (decadal time scale) and a trend which may be due to GHG forcing. Moreover, future extrapolations of the GHG forced temperature trend show a magnitude which is similar to GCM projections. This holds even for the seasonal and latitudinal patterns of past and future global temperature change. Both methods, however, imply considerable uncertainties. From the statistical point of view most important may be the alternative possibilities of other than GHG forcing leading not only to alternative reproductions of observed climate change but also to uncertainties in the future extrapolation. Not all possible forcing is included in our statistical model as for instance stochastic forcing (Wigley and Raper, 1991) or cooling by anthropogenic sulfate concentrations in the troposphere (Schlesinger *et al.*, 1992; Wigley and Raper, 1992). Just in cooling due to a long–term increase of tropospheric sulfate concentrations may explain another discrepancy between deterministic GCM and statistical modelling. So, it is possible that mankind has increased the global mean surface air temperature by as much as roughly 1 K until nowadays.

Acknowledgements

This work was supported by the German Government Climate Research Programme (BMFT, Project number 07 KFT 16/5). Most figures were drawn by C. Lidzba. We are very grateful for this support.

REFERENCES

Angell, J. K., 1988. Variations and trends in tropospheric and stratospheric global temperatures, 1958-87. *J. Clim.*, **1**, 1296-1313; 1992: priv. comm.

Augustsson, T., and V. Ramanathan, 1977. A radiative–convective model study of the CO_2 climate problem. *J. Atmos. Sci.*, **34**. 448-451.

Cress, A., and C.-D. Schönwiese, 1992. Statistical signal and signal–to–noise assessments of the seasonal and regional patterns of global volcanism–temperature relationships. *Atmósfera*, **5**, 31-46 (1990:detailed Report in German).

Cubasch, U., K. Hasselmann, H. Höck, E. Maier–Reimer, U. Mikolajewicz., B. D. Santer, and R. Sausen, 1991. Time–dependent greenhouse warming computations with a coupled ocean–atmosphere model. Report No. 67, Max–Planck–Institut für Meteorologie, Hamburg, FRG; *Clim. Dyn.*, **8**, 55-69 (1992).

Dai, J., 1992. pers. comm.

Eddy, J. A., 1967. The Maunder minimum. *Science*, **192**, 1189-1202.

Eddy, J. A., R. L. Gilliland, and D. V. Hoyt, 1982. Changes in the solar constant and climatic effects. *Nature* , **330**, 689-693.

Foukal, P. V. and J. Lean, 1990. An empirical model of total solar irradiance variation between 1874 and 1988. *Science*, **247**, 556-558.

Friis–Christensen, E., and K. Lassen, 1991. Length of the solar cycle: An indicator of solar activity closely associated with climate. *Science*, **254**, 698-700.

Gilliland, R. L. 1982. Solar, volcanic, and CO)2 forcing of recent climatic changes. *Climatic Change*, **4**, 111-131.

Hammer, C. U., H. B. Clausen, and W. Dansgaard, 1980. Greenland ice sheet evidence of post–glacial volcanism and its climatic impact. *Nature*, **288**, 230-235.

Hansen, J., D. Johnson, A. Lacis, S. Lebedeff, P. Lee, D. Rind, and G. Russel, 1981. Climate impact of increasing atmospheric carbon dioxide. *Science*, **213**, 957-966.

Hansen, J. and S. Lebedeff, 1987. Global trends of measured surface air temperature.*J. Geophys. Res.*, **92 (D11)**, 13345-13372; 1993: priv. comm.

Hansen, J., I. Fung, A. Lacis, D. Rind, S. Lebedeff, R. Ruedy, and G. Russell, 1988. Global climate changes as forecast by Goddard Institute for Space Studies three–dimensional model. *J. Geophys. Res.*, **93(D8)**, 9341-9364.

Houghton, J. T., G. J. Jenkins, and J. J. Ephraums, 1990. Climate Change. The IPCC Scientific Assessment. Cambridge Univ. Press, Cambridge, 365 p.

Houghton, J. T., B. A. Callandar, and S. K. Varney, 1992. Climate Change 1992. The Supplementary Report to the IPCC Scientific Assessment. Cambridge Univ. Press, Cambridege, 200 p.

Hoyt, D. V., 1979. Variations in the solar constant caused by changes in the active features on the sun. In McCormac, B. M., and T. A. Seliga, eds.: Solar–Terrestrial Influences on Weather and Climate. Reidel, Dordrecht, pp. 65-68.

Jacoby, G. C., and R. D'Arrigo, 1989. Reconstructed Northern Hemisphere annual temperature since 1671 based on high latitude treering data from North America. *Climatic Change*, **14**, 39-59.

Jones, P. D., T. M. L. Wigley and P. M. Kelly, 1982. Variations in surface air temperatures: Part 1. Northern Hemisphere, 1881-1980. *Mon. Weath. Rev.*, **110**, 59-70.

Jones, P. D., T. M. L. Wigley, and G. Farmer, 1991. Marine and land temperature data sets: a comparison and a look at recent trends. In M. E. Schlesinger (ed.): Greenhouse–Gas–Induced Climatic Change: A Critical Appraisal of Simulations and Observations. Elsevier, Amsterdam, pp 153-172; 1992: priv. comm.

Jones, P. D., 1991. Climate Research Unit, University of East Anglia, Norwich. In NASA Climate Data System Staff, 1992: Greenhouse effect detection experiment. Selected data sets for greenhouse effect research. CD ROM Disc 1.

Keeling, D. C., 1982. Measurements of the concentration of carbon dioxide at Mauna Loa Observatory, Hawaii. In W. C. Clark (ed.): Carbon Dioxide Review 1982. Clarendon, Oxford, pp. 377-385; 1985 ... 1992: priv comm. see also Carbon Dioxide Information and Analysis Center (CDIAC), Oak Ridge, updates and climatic data on magnetic tape.

Kondratyev, K. Y., and G. A. Nikolsky, 1970. Solar radiation and solar actvity. *Quart. J. Roy. Meteor. Soc.*, **96**, 509-522.

Labitzke, K., B. Naujokat, and J. K. Angell, 1986b. Long–term temperature trends in the middle stratosphere of the Northern Hemisphere. *Adv. Space Res.*, **6**, 7-16; 1992: priv. comm.

Lamb, H. H., 1970. Volcanic dust in the atmosphere; with a chronology and assessment of its meteorological significance. *Phil. Transactions R. Met. Soc.*, **A266**, 425-533.

Lamb, H. H., 1983. Update of the chronology of assessments of the volcanic dust veil index. *Climate Monitor*, **12**, 79-90.

Landscheit, T., 1988. Solar rotation, impulses of the torque in the sun's motion, and climatic variation. *Climatic Change,* **12**, 265-295.

Lee, R. B., B. R. Barkstrom, E. F. Harrison, M. A. Gibson, S. M. Natarajan, W. L. Edmonds, A. T. Mecherikunnel, and H. L. Kyle, 1988. Earth radiation budget satellite extraterrestrial solar constant measurements: 1986-1987 increasing trend. *Adv. Space Res.*, **8**, 11-13; 1990: priv. comm.

Lindzen, R. S., 1990. Some coolness concerning global warming. *Bull. Amer. Meteor. Soc.*, **71**, 288-299.

Malcher, J. and C.-D. Schönwiese, 1987. Homogeneity, spatial correlation and spectral variance analysis of long European and North American air temperature records. *Theor. Appl. Climatol.*, **38**, 157-166.

Miles, M. K., P. B. Gildersleeves, 1987. A statistical study of the likely causative factors in the climatic fluctuations of the last 100 years. *Met. Mag.*, **106**, 314-322.

Neftel, A., E. Moor, H. Oeschger, and B. Stauffer, 1985. Evidence from polar ice cores for the increase in atmospheric CO_2 in the past two centuries. *Nature*, **315**, 45-47.

Robock, A. 1979. The "Little Ice Age": Northern Hemisphere average observations and model calculations. *Science*, **206**, 1402-1404.

Robock, A., 1991. The volcanic contribution to climate change of the past 100 years. In M. E. Schlesinger (ed.): Greenhouse–Gas–Induced Climatic Change: A Critical Appraisal of Simulations and Observations. Elsevier, Amsterdam, pp. 429-443.

Sausen, R., K. Hasselmann, E. Maier–Reimer, R. Voss, 1992. On the cold start problem in transient simulations with coupled atmosphere–ocean models. Report No.83, Max–Planck–Institut für Meteorologie, Hamburg, FRG.

Schlesinger, M. E., X. Jiang, and R. J. Charlson, 1992. Implication of anthropogenic atmospheric sulphate for the sensitivity of the climate system. In Rosen, L., and R. Glasser, eds.: Climate Change and Energy Policy. Am. Inst. Physics, New York, pp. 75-108.

Schneider, U., and C.-D. Schönwiese, 1989. Some statistical characteristics of El Niño/southern oscillation and North Atlantic oscillation indices. *Atmósfera*, **2**, 167-180.

Schönwiese, C.-D., 1983. Northern Hemisphere temperature statistics and forcing. part A: 1881-1980 AD. *Arch. Met. Geophy. Biocl., Ser. B*, **32**, 337-360.

Schönwiese, C.-D., 1988a. Volcanic activity parameters and volcanism–climate relationships within the recent centuries. *Atmósfera*, **1**, 141-156.

Schönwiese, C.-D., 1988b. Volcanism and air temperature variations in recent centuries. In Gregory, S.: Recent climatic change. Belhaven Press, London, pp 20-29.

Schönwiese, C.-D., and K. Runge, 1991. Some updated statistical assessments of the surface temperature response to increase greenhouse gases. *Int. J. Climatol.*, **11**, 237-250.

Schönwiese, C.-D., 1991. A statistical hypothesis on global greenhouse–induced temperature change. *Theor. Appl. Climatol.*, **44**, 243-245.

Schönwiese, C.-D., and U. Stähler, 1991. Multiforced statistical assessment of greenhouse–gas–induced surface air temperature change 1890-1985. *Climate Dyn.*, **6**, 23-33; detailed Repot in German.

Schönwiese, C.-D., 1992. Variation statistics and natural as well as greenhouse forcing of the mean Northern Hemisphere air temperature within the recent c. 400 years. In T. Mikami (ed.): Proceedings of the Internat. Symp. Little Ice Age Climate, Tokyo Metropol. Univ., pp 314-319.

Schönwiese, C.-D., R. Ullrich, and F. Beck, 1992. Solare Einflüsse auf die Lufttemperaturvariationen der Erde in den Ietzten Jahrhunderten. Bericht No. 92, Institut für Meteorolgie u. Geophysik d. Univ. Frankfurt/Main, 215 p.

Schönwiese, C.-D., R. Ullrich, F. Beck, and J. Rapp, 1994. Solar Signals in Global Climatic Change. *Climatic Change*, **27**, 259-281.

Schönwiese, C.-D., 1994. Analysis and prediction of global climate temperature change based on multiforced observational statistics. *Environm. Poll.*, **83**, 149-154.

Simkin, T., L. Siebert, L. McClelland, D. Bridge, C. Newhall, and J. H. Latter, 1981. Volcanoes of the World. Smithsonian Institution. Hutchinson, Stroudsburg, 236 p.

Simkin, T., L. McClelland, M. Summers, E. Nielsen, and T. C. Stein (eds.), 1989. Gobal volcanism 1975-1985. American Geophysical Union, Washington, DC, 655 p.

Vinnikov, K., P. Y Groisman, and K. M. Lugina, 1990. Empirical data on contemporary global climate changes (temperature and precipitation). *J. Climate*, **3**, 662-677.

Wigley, T. M. L., and S. C. B. Raper, 1991. Internally generated natural variability of global–mean temperatures. In Schlesinger, M. E., ed.: Greenhouse–Gas–Induced Climatic Change: A Critical Appraisal of Simulations and Observations. Elsevier. Amsterdam, pp 471-482.

Wigley, T. M. L., and S. C. B. Raper, 1992. Implications for climate and sea level of revised IPCC emission scenarios. *Nature*, **357**, 293-300.

Wright, P. B., 1984. Relationship between indices of the southern oscillation. *Mon. Weath. Rev.*, **112**, 1913-1919.